



**HAL**  
open science

# Theoretical determination of adsorption and ionisation energies of polycyclic aromatic hydrocarbons on water ice

Eric Michoulier, Nadia Ben Amor, Mathias Rapacioli, Jennifer Anna Noble, Joëlle Mascetti, Céline Toubin, Aude Simon

► **To cite this version:**

Eric Michoulier, Nadia Ben Amor, Mathias Rapacioli, Jennifer Anna Noble, Joëlle Mascetti, et al.. Theoretical determination of adsorption and ionisation energies of polycyclic aromatic hydrocarbons on water ice. *Physical Chemistry Chemical Physics*, 2018, 20, pp.11941-11953. 10.1039/C8CP01175C . hal-01764650

**HAL Id: hal-01764650**

**<https://hal.science/hal-01764650>**

Submitted on 18 Jul 2024

**HAL** is a multi-disciplinary open access archive for the deposit and dissemination of scientific research documents, whether they are published or not. The documents may come from teaching and research institutions in France or abroad, or from public or private research centers.

L'archive ouverte pluridisciplinaire **HAL**, est destinée au dépôt et à la diffusion de documents scientifiques de niveau recherche, publiés ou non, émanant des établissements d'enseignement et de recherche français ou étrangers, des laboratoires publics ou privés.

# Theoretical determination of adsorption and ionisation energies of polycyclic aromatic hydrocarbons on water ice

Eric Michoulier,<sup>†,§</sup> Nadia Ben Amor,<sup>‡</sup> Mathias Rapacioli,<sup>‡</sup> Jennifer A. Noble,<sup>†</sup>  
Joëlle Mascetti,<sup>¶</sup> Céline Toubin,<sup>†</sup> and Aude Simon<sup>\*,‡</sup>

<sup>†</sup>*Lab. Phys. Lasers Atomes & Mol., Univ. Lille 1 & CNRS, UMR 8523, F-59655  
Villeneuve D'Ascq, France.*

<sup>‡</sup>*Lab. Chim. & Phys. Quant. LCPQ IRSAMC, Univ. Toulouse [UPS] UPS & CNRS,  
UMR5626, 118 Route Narbonne, F-31062 Toulouse, France.*

<sup>¶</sup>*Institut des Sciences Moléculaires (ISM), Université de Bordeaux & CNRS, UMR 5255,  
351 Cours de la Libération, F-33405 Talence, France.*

<sup>§</sup>*current address: Lab. Chim. & Phys. Quant. LCPQ IRSAMC, Univ. Toulouse [UPS]  
UPS & CNRS, UMR5626, 118 Route Narbonne, F-31062 Toulouse, France.*

E-mail: [aude.simon@irsamc.ups-tlse.fr](mailto:aude.simon@irsamc.ups-tlse.fr)

Phone: +33 (0)5 61 25 88 73

## Abstract

In dense interstellar media, Polycyclic Aromatic Hydrocarbons (PAHs) are likely to condense onto or integrate into water ice mantles covering dust grains. Understanding the role of ice in the photo-induced processes involving adsorbed PAHs is therefore a current key issue in astrochemistry. This implies beforehand -(i)- the knowledge of PAH-ice interactions, *i.e.* PAH-ice adsorption energies and local structure at the PAH-ice interface, as well as -(ii)- the understanding of the fate of electrons in the PAH-ice system upon excitation. Regarding -(i)-, in this work, we determined the lowest energy structures of PAH-ice systems for a variety of PAHs ranging from naphthalene to ovalene on three types of ices, crystalline (Ih and Ic) and amorphous (low density), using an explicit description of the electrons and a finite-size system. The electronic structure was determined using the Self Consistent Charge Density Functional based Tight Binding (SCC-DFTB) scheme with modified Mulliken charges in order to insure a good description of the studied systems. Regarding -(ii)-, the influence of the interaction with ice on the Vertical Ionization Potentials (VIPs) of the series of PAHs was determined using the constrained SCC-DFTB scheme, that was benchmarked against correlated wavefunction results for PAH(H<sub>2</sub>O)<sub>n</sub> (n=1-6,13) clusters. The results show a deviation smaller than  $\sim 1.4$  eV of the VIPs of PAH adsorbed on ice with respect to the gas phase values. This is discussed in the light of experimental results and other theoretical data.

## 1 Introduction

Polycyclic Aromatic Hydrocarbons (PAHs) have received considerable interest in astrochemistry since they were proposed, in the mid-eighties, as the carriers of the Aromatic Infrared Bands (AIBs), a set of mid-IR emission bands observed in many regions of the interstellar medium.<sup>1,2</sup> This “Astro-PAH” population would constitute a reservoir of interstellar carbon as it is generally admitted that they would contain about 10 to 20 percent of the total

elementary carbon.<sup>3,4</sup> However, despite a longstanding synergy between astronomical observations and laboratory investigations, no specific PAH molecule has been identified yet.<sup>5</sup> Astro-PAHs may also play an important role in the chemistry of the interstellar medium. A current important topic is the investigation of astro-PAH energetic processing (see Simon and Rapacioli<sup>6</sup> and references therein), which involves studies aiming at probing the possible relationship between astro-PAHs and recently observed carbonaceous molecules such as fullerenes,  $C_{60}$ <sup>7,8</sup> and  $C_{60}^+$ ,<sup>9,10</sup> and at investigating the potential catalytic role of astro-PAHs in the formation of  $H_2$ ,<sup>11-13</sup> the most abundant molecule in space.

In dense interstellar clouds, where temperatures are low ( $< 50$  K), molecular PAHs may condense onto or integrate into icy mantles on dust grains.<sup>14</sup> As explained hereafter, both spectroscopic diagnostics for their presence, and their photoprocessing, are expected to be different from that of the gas phase.

First, let us specify that the precise structure of interstellar ice remains unclear, although it is generally agreed that it is amorphous upon formation.<sup>15</sup> Indeed, on dense clouds, water ice can be detected by its IR absorption band at  $3.1 \mu\text{m}$ , assigned to the OH-stretching mode, that has been shown to be broad and largely featureless.<sup>16</sup> PAHs condensed on or integrated in ice are also identified by their IR absorption spectra,<sup>17-19</sup> IR emission being quenched by non-radiative relaxation channels such as energy transfer into the phonons of the grain. For instance, the  $3.3/3.25 \mu\text{m}$  feature in icy dust environments was assigned to aromatic C-H stretch.<sup>20,21</sup> This motivated experimental investigations of the absorption IR spectra of PAHs in water ice.<sup>22-24</sup> In such experiments, the assignment of the bands is difficult because first, the PAH's bands and those of water ice fall in the same domain and second, the PAH is diluted in the water ice, therefore leading to weaker bands than that assigned to water. UV irradiation or energetic particle collisions of dust surface in space may lead to energetic processes that will modify the chemistry at the surface of grains.<sup>25</sup> This motivated, in particular, experimental studies dedicated to the investigations of the photoprocessing of

PAHs in water ices after UV irradiation in different conditions (energy of incident photons, temperature...). At VUV high energy (light distribution centered at 121.6 nm and 160 nm, ) irradiation, it seems that the dominant process at low temperature is the formation of PAH cations,<sup>26–28</sup> but also that photochemistry is initiated, involving PAH oxidation in particular.<sup>28</sup> When increasing temperature, a richer photochemistry occurs, leading to formation of alcohols, quinones and ethers,<sup>26,29,30</sup> with the observation of regiochemistry<sup>30</sup> and this could considerably influence the inventory of aromatics in meteorites. At lower energy ( $\lambda > 235$  nm), UV photochemistry of pyrene and coronene adsorbed on and embedded in Amorphous Solid Water (ASW) at 10 K<sup>31,32</sup> also revealed the production of oxygen-containing PAH products. This reactivity occurs at energies below the ionization energy of bare PAHs ( $\sim 7.4$  and  $7.2$  eV for pyrene and coronene respectively) and a current key issue is to understand the mechanism for this photochemistry in solid state.

A hypothesis is that photoreactivity, even at lower energy, could be ion-mediated,<sup>28</sup> motivating computational studies on the influence of ice on the ionization energy of PAHs. Experimental investigations combined with computational studies have shown that the ionization of PAHs adsorbed on water ice requires about 1.5 to 2.0 eV less energy than the gas phase ionization energies of PAHs,<sup>33,34</sup> and that the formed PAH radical cations would be particularly stable over time.<sup>35</sup> That could be accounted for by the fate of the released electrons that would not be free electrons but would attach to H<sub>2</sub>O molecules or free radicals such as OH formed during the ice photolysis.<sup>35</sup> Theoretical studies estimated the electron affinity of water ice in the 1.65–3.3 eV range<sup>36</sup> (Density Functional Theory (DFT) study of water clusters and extrapolation law to infinite size) and that of OH trapped in ice at 5.06 eV<sup>34</sup> (using the isodensity polarized continuum model). Overall, the physical and chemical processes behind the PAH ionization energy lowering in water ice compared to that of PAHs in the gas phase have not been fully understood and further experimental and theoretical studies are needed.<sup>35</sup> This study enters this framework. It proposes a new modeling with quantal description of the electrons to investigate the influence of adsorption of ice on the

PAH ionisation energy.

Describing PAH-water ice systems with a quantum description of the electrons is a challenge due to the size of the system that has to be described to provide realistic data. To the best of our knowledge, very few studies have been undertaken in this framework. For instance, the influence of a water ice environment on the electronic absorption and emission spectra of pyrene has recently been studied through *ab initio* simulations for a DFT optimized structure of pyrene surrounded by about forty water molecules.<sup>37</sup> Electronic spectra of benzene adsorbed on water ice have been computed with the Time-Dependent DFT method modeling the system within a model combining DFT and force field.<sup>38</sup> The authors highlighted the relationship between the interface structure (dangling OH), interaction energies and electronic spectra.<sup>38</sup>Very recently, Michoulier et al.<sup>39</sup> studied the adsorption of a series of PAHs on various water ice surfaces using a molecular dynamics/force field approach. They established correlation laws between the adsorption energies and the number of dangling OH bonds interacting with the PAH. As far as we know, no study of the influence of ice on the ionisation potential of PAHs, with all valence electrons of the systems described explicitly, has been undertaken so far. As explained in next section, this is a challenge as DFT-based approaches overestimate charge delocalization due to self-interaction errors.<sup>40</sup>

We present in this paper a modeling of PAHs adsorbed on water ice, with an explicit description of the electrons within the Self Consistent Charge Density Functional based Tight Binding (SCC-DFTB) scheme.<sup>41-43</sup> This work follows the molecular dynamics/force-field studies<sup>39</sup> that provided us with the initial structures of the PAH:water ice systems investigated in the present paper, that is to say a series of PAHs ranging from benzene to ovalene, adsorbed on three types of ices, amorphous (LDA for Low Density Amorphous), and crystalline (Ih and Ic). Structures, interaction energies and ionisation potentials were computed using the approaches described in Section 2. The results are reported and discussed in Section 3.

## 2 Computational approach

### 2.1 Electronic structure

In this work, we have used the second order version of DFTB, also known as Self Consistent Charge SCC-DFTB,<sup>43</sup> using the mio-set of parameters,<sup>43</sup> and the dispersion correction as reported in ref.<sup>44</sup> All DFTB calculations were performed using the deMonNano code<sup>45</sup> where several modifications of the SCC-DFTB potential to describe neutral and charged molecular complexes and clusters<sup>46</sup> can be found. In the SCC-DFTB scheme, the potential is expressed as a function of atomic charge fluctuations and in the original scheme, these charges are Mulliken charges. In this model, the electrons occupying two atomic orbitals based on different atoms are equally shared between the latter for the calculation of their atomic charges whatever the atomic electronegativity difference is. To improve bond polarity description, we used in our previous studies<sup>44</sup> the Charge Model 3 (CM3) approach<sup>47</sup> instead of Mulliken charges in the DFTB energy expression in order to describe PAH-water interactions and water-water interactions. From a general point of view, the use of CM3 charges enabled us to improve the description of bond polarities and therefore the treatment of long-range electrostatic interactions<sup>44</sup> and the values of IR intensities.<sup>48</sup> Good results were also obtained for intermolecular binding energies within PAH-water and water clusters.<sup>49,50</sup> Using these charges, we further investigated the conformational dynamics<sup>51</sup> and heat capacities<sup>52</sup> of water clusters adsorbed on PAHs. Finally, the stability, energetics and IR spectra of water-PAH clusters embedded in a rare gas matrix were determined using a mixt DFTB/force field approach, the water-PAH clusters being described with DFTB and CM3 charges.<sup>53</sup>

In order to improve computational efficiency, we present a simpler alternative to CM3 charges by introducing a non-symmetric bias directly in the Mulliken repartition of the overlapping density:

$$\phi_\mu(r)\phi_\nu(r) \simeq \frac{1}{2}S_{\mu\nu}((1 + t_{\mu\nu})|\phi_\mu(r)|^2 + (1 - t_{\mu\nu})|\phi_\nu(r)|^2) \quad (1)$$

where  $t_{\mu\nu}$  is a free parameter between -1 and +1 (0 being equivalent to Mulliken charges), expressing the polarity of a bond, in the same philosophy as the empirical parameters used to compute CM3 charges, although not strictly equivalent. In the following,  $t_{\mu\nu}$  is determined empirically as an atomic pair parameter ( $t_{\mu\in A,\nu\in B} = t_{AB}$ ). This scheme is called hereafter the Weighted Mulliken (WMull) scheme. The  $t_{O-H}$  parameter was determined so as to reproduce the water dimer structure and interaction energy obtained both with CM3 charges determined in ref<sup>49</sup> and correlated wavefunction calculations.<sup>54</sup> We obtained a value of  $t_{O-H}=0.39$ . We checked that the interaction energies of larger water clusters were also well reproduced (see Figure S1), the difference with wavefunction approaches increasing with cluster size, and reaching a maximum discrepancy (for the "10-PP2" cluster) of 1.63 kcal/mol (6.83kJ/mol), corresponding to a relative error of 1.76%. The  $t_{C-H}$  and  $t_{OC}$  values were adjusted to reproduce the structures and interaction energies of  $PAH(H_2O)$  clusters (see Table S1). Final  $t_{AB}$  values of 0.08 and 0.30 for O-C and C-H respectively, reproducing the energies obtained with CM3 charges by less than 0.1 kJ.mol<sup>-1</sup>, were retained.

The SCC-DFTB potential with WMull charges and dispersion interactions will be used to compute the electronic structure of PAH-ice systems as described in next section. We will refer to this potential as simply DFTB in the following. It should be pointed out that a good agreement is found between experimental and DFTB ionisation potentials, vertical and adiabatic (respectively VIP and AIP), for the series of PAHs, with a maximum difference of 0.09 eV (VIP) and 0.14 eV (AIP) (see Figure S2).

A standard DFTB calculation of charged clusters is not physically correct as the charge delocalization among all monomers is overestimated<sup>55</sup> due to self interaction errors.<sup>40</sup> It results in our case in an overestimation of the charge carried by water molecules and an underestimation of ionization potentials. To circumvent this problem, we used the charge-constrained DFTB approach (C-DFTB)<sup>56,57</sup> constraining the charge to be localized on the



PAH, to compute VIPs. In order to validate this approach, we first computed the IPs of pyrene solvated by water clusters  $(\text{H}_2\text{O})_n$  (with  $n=1-6$  and 13), the latter structure ( $n=13$ ) being extracted from a pyrene-water ice structure (see next section). The C-DFTB/DFTB VIPs values were compared to MP2 VIPs, obtained for the DFTB geometries, using the ANO basis set<sup>58</sup> and the 7.8 MOLCAS package.<sup>59-61</sup> This benchmark is presented in section 3.1.

## 2.2 Determination of minimum energy structures

We distinguish the case of PAHs interacting with small water clusters, which are used to benchmark the C-DFTB approach, and PAHs interacting with ice, which are the final systems of interest.

### $\text{C}_{16}\text{H}_{10}(\text{H}_2\text{O})_n$ clusters

The DFTB structures of  $\text{C}_{16}\text{H}_{10}(\text{H}_2\text{O})_n$  clusters ( $n=1,6$ ) were obtained using Molecular Dynamics Parallel Tempering<sup>62</sup> (MDTP) followed by gradient quenching to reach minima, as explained in a previous work.<sup>63</sup> In this work, MDPT simulations of 0.5 ns were ran for 40 temperatures ranging from 30 to 300 K, with an exponential distribution of temperatures, and replica exchanged tried every 100 fs. A Nose Hoover thermostat chain of five thermostats with frequencies of  $800 \text{ cm}^{-1}$  was used. In order to avoid evaporation, we applied a rigid spherical potential centered on the cluster center of mass defined in Hartree by  $V(r) = 0.008(r - r_0)^4$  with  $r_0 = 8 \text{ \AA}$ . To obtain the low-lying energy minima, we proceeded as follows: for a selection of 5 temperatures (30, 99, 168, 238 and 300 K), we optimized with conjugated gradient a selection of 65 structures for each temperature (total of 325 structures optimized). We used the most stable ones to compute vertical C-DFTB and MP2 ionisation potentials.

We must specify that a third, intermediate system, consisting of pyrene interacting with a small waters cluster extracted from pyrene-LDA ice systems, was used for additional bench-

mark (see section 3.1 hereafter)

### PAH-ice systems

Our goal is to determine good model finite-size systems for PAH-ice, tractable by DFTB and MD/DFTB. The initial geometries were extracted from the PAH-ice structures determined by Michoulier et al.<sup>39</sup> using a MD/FF approach. These authors determined the lowest energy configurations for various PAHs ranging from benzene to ovalene adsorbed on ice (LDA, Ih and Ic) surfaces. More precisely, for each PAH-ice duet, the final frames of 50 MD/FF trajectories have been used as starting geometries for the DFTB calculations. Finite-size systems, tractable with DFTB, were elaborated following the procedure detailed hereafter: we build a cluster of water molecules in interaction with the PAH, consisting of an inner shell (delimited by radius  $R_1$ ) and an outer shell (of radius  $R_2$  larger than  $R_1$ ). The PAH and all molecules of the cluster are considered for the DFTB energy/gradient calculation but the water molecules from the outer shell are kept frozen during MD/geometry optimization. For a given water molecule, we define the metric  $d(\text{C-O})$  as the minimum distance between its oxygen atom and any of the PAH carbon atoms. A water molecule is considered to belong to the inner shell if  $d(\text{C-O})$  is smaller than  $R_1$  and outer if  $d(\text{C-O})$  is larger than  $R_1$  and smaller than  $R_2$ .

We now discuss the choice of  $R_1$  and  $R_2$ .

- The thickness of the layer of frozen molecules  $R_2-R_1$  was determined so that the mobile water molecules are coordinated to at least one water molecule from the outer shell. With this constraint, a thickness of  $R_2-R_1=3.5 \text{ \AA}$  was found. It corresponds to the distance between the first and the second solvation shell of the O-O radial distribution function (see ref.<sup>39</sup> for instance). This layer allows to maintain the molecular density of the FF structure.
- The  $R_1$  value was determined so as to obtain quasi convergence for PAH-ice interaction energies, the thickness of the second layer being fixed to  $3.5 \text{ \AA}$  (see Figure S3). A value of  $7 \text{ \AA}$  was chosen for  $R_1$  since it gives a good compromise between convergence and computational

cost. The  $R_2$  value is then equal to  $10.5 \text{ \AA}$ . Using these radii, the minimum size reproducing the FF pyrene-water ice binding energy amounts to about 50 water molecules allowed to relax, and 90 frozen molecules (more precisely 55 mobile/94 frozen for LDA ice and 51 mobile /92 frozen for Ih, which are averaged values over the 50 configurations).

### 3 Results and discussion

In this section, we first present the benchmark studies for  $C_{16}H_{10}(H_2O)_n$  (section 3.1), and secondly the structures, interaction energies and IPs of PAHs on ice (section 3.2).

#### 3.1 Pyrene solvated by water clusters

The geometries of the clusters  $(C_{16}H_{10})(H_2O)_n$  ( $n=1-6$ ) obtained from MDPT/quenching calculations, are reported in Figure 1. Using these geometries, VIPs were computed at the DFTB, C-DFTB and MP2/(ANO-L 3s2p1d (C) / 2s1p (H)) levels of theory. The values are reported in Figure 1, along with the partial charge of pyrene with the unconstrained DFTB approach (in parenthesis). Knowing that the VIP of pyrene is found at 7.41 (resp. 7.40 eV) at the DFTB (resp. MP2//DFTB) levels of theory, we may notice that the effect of the adsorption of water cluster on the IP of pyrene tends to increase slightly the IP, but that the perturbation is small (+0.49 eV max regarding MP2 results, obtained for  $n=3$ ). Secondly, we may say that the agreement between C-DFTB and MP2 results is very satisfactory, the discrepancy ranging from 0.01 ( $n=1$ ) to 0.11 eV ( $n=5$ ), the IPs at the C-DFTB level being lower than that at the MP2 level. Regarding unconstrained DFTB results, the IPs are lower than the MP2 ones by 0.01 ( $n=1$ ) to 0.23 eV ( $n=5$ ) and the larger the water clusters the larger the discrepancy. As expected, the partial charge on the PAH ranges from 0.91 to 0.75 ( $n=5$ ), overall decreasing when the cluster size increases. This was expected due to the overstabilization of the charged delocalized forms in standard DFT and DFTB.

The trends obtained for  $(C_{16}H_{10})(H_2O)_n$  ( $n=1-6$ ), in particular the small IP perturbation of

the PAH upon hydration, and the better agreement between MP2 and C-DFTB results than between MP2 and DFTB results, were confirmed studying a cluster with 13 water molecules obtained by truncation of the optimized geometry of pyrene on LDA ice (see Figure 1, bottom). The effect of the constraint is more significant for this cluster than for smaller clusters : the IP of the PAH is underestimated by 0.40 eV (DFTB) *vs* 0.04 eV (C-DFTB) with respect to MP2 results, with the partial charge on the PAH amounting to 0.57 with pure DFTB. These results legitimate the use of C-DFTB to compute the IPs of PAH on ice.

For PAH-water clusters systems, the slight increase of the PAH VIP can be understood, because in the stable geometry of the neutral cluster, the H atoms of the water molecules interacting with the PAH point towards the PAH. Such a configuration is unfavourable for the cation, the H atoms bearing a slightly positive charge leading to a repulsive interaction with the global positive charge of the PAH. We also optimized locally the geometries of the  $(C_{16}H_{10})(H_2O)_n^+$  ( $n=1-6$ ) molecular ions using the C-DFTB potential (these are reported in Figure S4). As expected, in these, the water molecules undergo rotation with respect to the neutral systems in order to interact with the  $PAH^+$  through their oxygen atoms. That was expected as these atoms bear a negative partial charges (-0.76e on the oxygen atom within the dimer  $PAH/H_2O$ ), hence their interaction with  $PAH^+$  has a stabilizing effect.

## 3.2 PAH on ice

### 3.2.1 Structures and interaction energies in neutral systems

The structures of the PAH-ice systems (PAH from benzene to ovalene on the three types of ice, Ih, Ic and LDA, 50 geometries for one duet PAH/ice) were optimized following the procedure explained in Section 2.2 with the starting point geometries extracted from the force-field geometries.<sup>39</sup> After the optimization, the structures are hardly modified and the relative orientation of the PAH with respect to the water-ice surface remains similar to the ones obtained from MD/FF simulations on PAH-ice systems<sup>39</sup> : the PAH remains parallel

to the surface or slightly bent as detailed in the previous work by Michoulier et al.<sup>39</sup> (range from 0 to 45 °). The 50 structures binding energies lie within about [-45,-86], [-56,-111], [-69, -111] kJ.mol<sup>-1</sup> in the case of pyrene adsorbed on LDA, Ih and Ic ice respectively. The geometries differ in particular from the PAH orientation with respect to the ice surface, and from the orientation of the surrounding water molecules. The most stable configurations for pyrene on the three types of ice are reported in Figure 2. As can be seen on this figure, in the most stable geometry, 4 H atoms of the water molecules point toward the PAH whereas, for the least stable, there is only one. The electron deficient H atoms of the water molecules at the ice surface (in average 0.38e) have a stabilizing interaction with the  $\pi$  cloud of the PAH. This is in line with the structures of PAH-water clusters obtained in section 3.1. This dependence of the interaction energies on the numbers of dangling O-H interacting with the PAH was previously shown by Sharma and co-workers in their study of benzene adsorbed on Ih ice with DFT/MM calculations.<sup>38</sup>

The PAH-ice interaction energies averaged over the 50 geometries, are reported in Figure 3, along with the values obtained with the GOCPAH (Gaseous Out of Plane Charges PAH) force field optimised by Michoulier et al.<sup>39</sup> for PAH-ice. The latter values, referred to as FF values in the following, were obtained after optimization with the corresponding FF of the relative position of the PAH with respect to the ice, starting from the same initial geometry as that taken for the DFTB calculations. The agreement between FF and DFTB values is very satisfactory. Indeed, RMSD values of 10 and 6 kJ.mol<sup>-1</sup> for Ih and LDA respectively with the GOCPAH force field were obtained, the DFTB values being systematically slightly above the FF values. This shows the consistency between the two approaches. We may also notice that our finite-systems' DFTB interaction energies are in very good agreement with the GOCPAH results that describe the infinite water-ice system (see Table 4 in ref.<sup>39</sup>).

Interestingly, as explained hereafter, the DFTB interaction energy for benzene/LDA

ice ( $-42 \text{ kJ mol}^{-1}$ ) is in excellent agreement with experimental values for the desorption of  $\text{C}_6\text{H}_6$  from compact ice. Adsorption energies were obtained from experimental data by fitting Temperature Programmed Desorption (TPD) curves<sup>64</sup> : with the so-called "Red-head" approach, a value of  $39 \text{ kJ mol}^{-1}$  was obtained,<sup>65</sup> while applying a fractional order "Polanyi-Wigner" (PW) fit to submonolayer TPD data led to an energy distribution of approximately  $41 \pm 0.5 \text{ kJ mol}^{-1}$ , covering the majority of the submonolayer regime.<sup>66</sup> A recent experimental study applied the PW method and obtained a value of  $40.6 \text{ kJ mol}^{-1}$ .<sup>67</sup> Let us mention that the desorption energy of  $\text{C}_6\text{H}_6$  from a compact amorphous ice surface in the laboratory is difficult to measure for a number of reasons. A critical point is that the  $\text{C}_6\text{H}_6:\text{C}_6\text{H}_6$  binding energy is greater than that of  $\text{C}_6\text{H}_6:\text{H}_2\text{O}$ , resulting in the preferential clustering of  $\text{C}_6\text{H}_6$  in so-called "islands" on the ice surface, even at submonolayer coverages.<sup>66</sup> As a result, it is difficult to measure the pure desorption energy of  $\text{C}_6\text{H}_6$  from water, as the experimentally-obtained value will be influenced by  $\text{C}_6\text{H}_6:\text{C}_6\text{H}_6$  interactions. It is difficult to directly compare these experimental values, given the different methods applied to the data to extract desorption energies. However, they are generally in very good agreement with each other and, most interestingly, with the DFTB value calculated here for the desorption of a single benzene molecule from an ice surface. The increase of the interaction energy (in absolute value) with the PAH size could be fitted by a first order dependence on the number of C and H atoms (see Figure 4). This allows to extrapolate the results to larger PAHs, that may become difficult to handle even with DFTB as it would imply the treatment of a too large ice slab.

### 3.2.2 Influence of the icy environment on IPs

Vertical ionization potentials of the optimized structures detailed in previous section (50 "configurations" for each PAH-ice duet) were computed with the C-DFTB approach. In the following, we only detail the studies performed with pyrene, the results for the other PAHs

are reported in the Supplementary Material.

The computed VIPs for pyrene adsorbed on water ice (Ih, Ic and LDA) for the 50 geometries of interest are reported in Figure 5 (see Figure S5 for the other PAHs). For each PAH-ice duet, the smallest and highest VIP among all 50 configurations, along with the maximum VIP variation and the VIP variation in the case of LDA ice, with respect to bare PAH, are reported in Table 1.

The first assessment is that the effect of adsorption on ice on the PAH ionization potential is small, with an overall largest VIP variation of -1.37 eV, corresponding to  $\Delta$  VIP Min. found for naphthalene on crystalline Ih ice (see Table 1). The largest VIP variations occur for crystalline Ih ice, followed by Ic ice. The largest amplitude of the VIP decrease ( $\Delta$  VIP Min. column in Table 1) is larger than that of the VIP increase ( $\Delta$  VIP Max. column in Table 1). Both  $\Delta$ VIP Min. and Max. absolute values seem to decrease as the PAH size increases. The minimum VIP variations correspond to the case of amorphous ice, which, for some configurations, does not lead to any change in the VIP (see last column of Table 1,  $\Delta$ VIP Max. (LDA) for anthracene, tetracene and ovalene in particular). However, as can be seen in Figure 5 and Figure S5, on average on all configurations, the adsorption on LDA clearly leads to a decrease of the VIP, but not more than  $\sim$ -0.8 eV. An important result is that the VIP variation is very dependent on the number of interactions between dangling H and the PAH (see Figure 6): the presence of dangling H interacting with the PAH favors an increase of the VIP. It can be understood as a partial positive charge of the dangling H destabilises the cationic pyrene. On the opposite, the interaction of O at the surface with the PAH (and in particular the H of the PAH, present when the PAH is bent at the surface), leads to a lowering of the IP. This can be generalized to all PAHs studied in this work (see Figure S6).

A correlation between the number of dangling OH which interact with the PAH and its VIP was made. We went further by investigating the linear correlation between  $E_{\text{int}}(\text{PAH}/\text{ice})$  and the VIPs. With the classical force field GOCPAH used in a previous

**Table 1: VIPs of PAHs adsorbed on water ice computed at the DFTB/C-DFTB level. The VIPs of bare PAHs are reported for comparison. The largest variations ( $\Delta$ VIPs Min. or Max.) are also reported, the last column referring to the LDA ice specifically. All values are expressed in eV.**

PAH	VIP Min. LDA/Ih/Ic	VIP Max. LDA/Ih/Ic	VIP bare PAH	$\Delta$ VIP Min.	$\Delta$ VIP Max.	$\Delta$ VIP Min./Max. (LDA)
Benzene	8.83/8.11/8.54	9.57/10.0/10.2	9.45	-1.34	+0.75	-0.62/+0.08
Naphthalene	7.48/6.82/7.50	8.12/8.92/8.70	8.19	-1.37	+0.73	-0.71/+0.07
Anthracene	6.77/6.27/6.57	7.39/8.11/8.12	7.40	-1.13	+0.72	-0.63/-0.01
Phenanthrene	7.10/6.65/7.00	8.01/8.56/8.45	7.83	-1.18	+0.73	-0.73/+0.18
Pyrene	6.70/6.15/6.54	7.56/8.07/8.02	7.41	-1.26	+0.66	-0.71/+0.15
Tetracene	6.22/5.79/6.20	6.84/7.54/7.41	6.87	-1.08	+0.63	-0.65/-0.03
Coronene	6.45/6.35/6.53	7.39/7.95/7.68	7.22	-0.87	+0.73	-0.77/+0.17
Ovalene	5.88/5.54/5.89	6.65/7.10/7.10	6.63	-1.09	+0.47	-0.75/+0.02

study,<sup>39</sup> it is possible to easily decompose  $E_{\text{int}}(\text{PAH}/\text{glace})$  as follows :

$$E_{\text{int}}(\text{PAH}/\text{ice}) = E_{\text{int}}(\text{H}_2\text{O}/\text{C} - \text{PAH}) + E_{\text{int}}(\text{H}_2\text{O}/\text{H} - \text{PAH}) \quad (2)$$

where  $E_{\text{int}}(\text{H}_2\text{O}/\text{C} - \text{PAH})$  (resp.  $E_{\text{int}}(\text{H}_2\text{O}/\text{H} - \text{PAH})$ ) corresponds to the interaction between the carbons (resp. hydrogens) of the PAH with all the water molecules of the system. Let us add that the geometries are those obtained after a DFTB optimization and thus these geometries were used for the calculation of the contributions  $E_{\text{int}}(\text{H}_2\text{O}/\text{C} - \text{PAH})$  and  $E_{\text{int}}(\text{H}_2\text{O}/\text{H} - \text{PAH})$ . A very good correlation is evidenced between VIP,  $E_{\text{int}}(\text{H}_2\text{O}/\text{C} - \text{PAH})$  and  $E_{\text{int}}(\text{H}_2\text{O}/\text{H} - \text{PAH})$  as shown in Figure 7. Indeed, if one extrapolates a linear law with the two interactions defined before,

$$\text{VIP} = a + b \times (E_{\text{int}}(\text{H}_2\text{O}/\text{H} - \text{PAH})) + c \times (E_{\text{int}}(\text{H}_2\text{O}/\text{C} - \text{PAH})) \quad (3)$$

the results obtained with the GOCPAH potential give a good superposition of the pyrene/ice VIPs and pyr/(H<sub>2</sub>O)<sub>n</sub> clusters (with  $a = 7.553 \text{ eV}$ ,  $b = 8.192 \cdot 10^{-3} \text{ eV.mol.kJ}^{-1}$  and  $c = 2.46 \cdot 10^{-3} \text{ eV.mol.kJ}^{-1}$ ). Note that the constant  $a$  (7.553 eV) is close to the DFTB VIP (7.410 eV). In Table 2, the different decompositions are reported for the four configurations



where the VIP is either increased or lowered for the pyr/(Ih or LDA) pairs. By viewing the linear law (equation 3), we observe that the sensitivity with respect to the interaction with the hydrogens of PAH is more important than with carbons. Moreover, when the number of free dangling OH is large, the value of  $E_{\text{int}}(\text{H}_2\text{O}/\text{C} - \text{PAH})$  becomes strongly negative. Conversely, when the VIP is the lowest, the interaction  $E_{\text{int}}(\text{H}_2\text{O}/\text{C} - \text{PAH})$  is positive. Both contributions  $E_{\text{int}}(\text{H}_2\text{O}/\text{C} - \text{PAH})$  and  $E_{\text{int}}(\text{H}_2\text{O}/\text{H} - \text{PAH})$  are necessary to correctly predict the behavior of the VIP as a function of the environment. We may note an enhanced deviation from the linear law for the pyr/LDA pair than for pyr/Ih and pyr/Ic.

**Table 2: Energy decomposition calculated with the GOCPAH model, the configurations were taken for the highest and lowest VIPs. These configurations correspond to the geometries of the figure 6.**

Configuration	$E_{\text{int}}(\text{H}_2\text{O}/\text{C} - \text{PAH})$ (kJ.mol <sup>-1</sup> )	$E_{\text{int}}(\text{H}_2\text{O}/\text{H} - \text{PAH})$ (kJ.mol <sup>-1</sup> )	VIP fit (eV)	VIP C-DFTB (eV)
IH conf 91	-199.8	110.4	8.0	8.1
IH conf 86	147.6	-201.0	6.3	6.1
LDA conf 19	-43.9	-35.2	7.2	7.6
LDA conf 36	63.1	-114.5	6.8	6.7

In this section, we have shown that there is a link between the number of dangling OH and the variation of the VIPs of the PAHs. In connection with this, a very good correlation between  $E_{\text{int}}(\text{PAH}/\text{ice})$ ,  $E_{\text{int}}(\text{H}_2\text{O}/\text{C} - \text{PAH})$  and  $E_{\text{int}}(\text{H}_2\text{O}/\text{H} - \text{PAH})$  has been determined. Such a good correlation exists with the VIP, whereas for this interpretation the interactions are calculated using a force field. A better correlation with the amorphous ice is expected if the force field used is polarizable.

The variation of the VIP due to the ice calculated in this work does not allow to explain the experimental results, as for instance those obtained for quaterrylene in amorphous water ice.<sup>33</sup> In that study, the energy needed to ionize quaterrylene would be lower by 2.11 eV in amorphous ice compared to the gas phase value whereas in our study, for the

largest PAH, ovalene, the maximum lowering of the VIP is only 0.7 eV. In the following, we first discuss the limitations of our model, and second, the reason why a simple ionization potential determination cannot allow to account for this experimental energy lowering of PAH ionization energy when adsorbed on or embedded into ice.

A main difference between our modeled PAH/ice systems and the experimental ones is that we only considered one interface whereas, in the experiments, PAHs are generally embedded in the ice. Additional calculations were therefore carried out with the structures resulting from MD/FF dynamics of solvated PAHs : the configurations are taken from NPT trajectories at atmospheric conditions. Freezing these MD/FF structures lead to LDA ice (ref ?), therefore finite-size systems were obtained from the latter and further optimized at the SCC-DFTB level following a similar procedure as that explained in Section 2.2. For each PAH, we have taken two solvated configurations where  $E_{\text{int}}(\text{PAH/liquid water})$  is minimal or maximal. Figure 8 represents two configurations extracted from DFTB calculations of solvated pyrene: the two configurations being characterized by a strong (**configuration 1**) and weak (**configuration 2**) interaction with the surrounding water molecules respectively. The corresponding structures for solvated ovalene are reported in Figure S7. In Table 3, all the results for the solvated PAHs with the two configurations 1 and 2 are summarized. Whatever the PAH, the VIP varies little, therefore total solvation in two extreme configurations does not reproduce the lowering of 2 eV that was observed experimentally.

For pyrene solvated in LDA, we obtained vertical IPs between 7.04 and 7.29 eV. These are decreased by 0.37 and 0.12 eV with respect to bare pyrene, which is even less than what we found for PAHs adsorbed at the surface. It is probably caused by important structural constraints due to water-water interactions that prevents the optimisation of the water-PAH interactions. Therefore a questionable description of the environment in our model does not seem to account for the discrepancy with experiments. Besides, in the experiments, during the irradiation, the local environment around the PAH may change,

**Table 3: VIPs and  $E_{\text{int}}(\text{PAH}/\text{water})$  for PAHs solvated with water. The calculations are performed at the DFTB level for interaction and C-DFTB for the VIP. The neutral geometries were optimized in DFTB.**

PAH	$E_{\text{int}}(\text{PAH}/\text{water})$		VIP		
	conf 1	conf2	conf 1	conf 2	isolated PAH
	(kJ.mol <sup>-1</sup> )		(eV)		
Benzene	-62	-94	8.72	9.17	9.45
Naphthalene	-80	-112	7.60	7.90	8.19
Anthracene	-128	-165	6.89	7.14	7.40
Phenanthrene	-120	-189	7.15	8.14	7.83
Pyrene	-152	-163	7.04	7.29	7.41
Tetracene	-157	-216	6.62	6.72	6.87
Coronene	-169	-234	6.88	7.34	7.22
Ovalene	-213	-296	6.38	6.45	6.63

and this is not taken into account in our study as only vertical IPs were computed. We may note that in the modeling by Woon and Park of PAHs embedded in ice,<sup>34</sup> the IP of benzene to pyrene is lowered by 2.1 - 1.5 eV, the lowering being smaller when increasing the size. This is done with a PCM (polarizable continuum model) and such lowering is not reproduced in the present study with a model with an explicit description of water molecules.

Another explanation, and the most plausible one, for the discrepancy with experiments, is that when the electron is ejected from the PAH, it is transferred to the ice. In experimental conditions, the electron can indeed recombine with water ice or radicals. To the best of our knowledge, the fate of the electrons in water ice is not fully understood and both further experimental and theoretical studies are needed.<sup>35</sup> Presently, a way to estimate the energy for PAH ionization on/in ice, assuming the electron is transferred to water ice, is to remove from the IP found in the present work the electron affinity of ice (1.65-3.5 eV), and this accounts for the ionization energy lowering found in experiments.<sup>35</sup> The characterization of a charge transfer state  $\text{PAH}^+-\text{H}_2\text{O}^-$  is a challenge with a DFTB hamiltonian, as  $\text{H}_2\text{O}^-$  is

not properly described. It is a current methodological issue that is out-of-the scope of this paper. Actually, it has recently been proposed that the charge transfer from the PAH to the ice is likely to occur through the population of excited states.<sup>68</sup> Such hypothesis is currently being checked by extensive multireference wavefunction calculations on PAH(H<sub>2</sub>O)<sub>n</sub> clusters and will be the object of a further publication.

## 4 Conclusion

In this work, we propose to model PAH on ice with an appropriate DFTB potential that includes modified Mulliken charges improving the description of bond polarities. The potential is validated on (H<sub>2</sub>O)<sub>n</sub> and PAH – H<sub>2</sub>O clusters. The PAH-ice systems are modeled using a finite-size approach benchmarked on results for infinite systems obtained with a dedicated optimized specific force field. The structures and interaction energies are in very good agreement. Due to the charge delocalization issue in DFTB, computing ionisation potentials for PAH-ice systems is not possible. We countered the problem using the C-DFTB approach to compute the electronic energy of the ionized PAH-ice system, constraining the charge to be localized on the PAH. The approach was first benchmarked computing vertical ionisation potentials of pyrene interacting with water aggregates and comparing the results with MP2 values. This showed that the use of the charge constraint was mandatory to obtain reliable IP values for PAH-ice systems. The small IP variation found with our calculations - maximum amplitude of  $\sim 1.4$  eV including all PAH-ice duet- does not appear sufficient to account for the energy lowering of 2 eV found in the experiment to ionize PAH adsorbed on ice, and this calls for further studies. This study is expected to have an impact in astrochemistry, in particular for astrochemical models of gas-grain interactions that need reliable input data.<sup>69</sup>

## Acknowledgement

This work has been funded by the Agence Nationale de la Recherche (ANR) project “PARCS” ANR-13-BS08-0005, with support from the French research network EMIE (Edifices Moléculaires Isolés et Environnés, GDR 3533 of CNRS). We acknowledge the computing facility CALMIP at the Paul Sabatier University in Toulouse. We also thank Jérôme Cuny and Fernand Spiegelman for helpful discussions.

## Supporting Information Available

Figure S1 : interaction energies within water clusters

Figure S2: VIPs for bare PAHs

Figure S3 : convergence of DFTB interaction energy as a function of the first shell radius

Figure S4 : geometries of pyrene-water clusters cations

Figure S5 : evolution of the VIP as a function of PAH-ice configuration for all studied PAHs and all ice types.

Figure S6: PAH-ice configurations leading to the smallest/highest VIP values for all studied PAH-ice duets.

Figure S7 : solvated ovalene configurations corresponding to min. and max. VIP.

Table S1 : interaction energies of water dimer and PAH-water dimers (benchmark)

## References

- (1) Allamandola, L. J.; Tielens, A. G. G. M.; Barker, J. R. Polycyclic Aromatic Hydrocarbons and the Unidentified Infrared-Emission Bands - Auto Exhaust Along the Milky-Way. *Astrophys. J.* **1985**, *290*, L25–L28.

- (2) Léger, A.; Puget, J. L. Identification of the 'unidentified' IR emission features of interstellar dust? *Astron. Astrophys.* **1984**, *137*, L5–L8.
- (3) Draine, B. T. Interstellar dust grains. *Annu. Rev. Astron. Astrophys.* **2003**, *41*, 241–289.
- (4) Joblin, C.; Léger, A.; Martin, P. Contribution of polycyclic aromatic hydrocarbon molecules to the interstellar medium. *Astrophys. J. Lett.* **1992**, *393*, L79–L82.
- (5) Joblin, C., Tielens, A. G. G. M., Eds. *EAS Publications Series*; EAS Publications Series; 2011; Vol. 46.
- (6) Simon, A.; Rapacioli, M. In *Chemical Modelling*; Joswig, J., Sprinborg, M., Eds.; SPR (Specialist Chemical Reports); Roy. Soc. Chem., 2017; Vol. 14; Chapter Energetic Processing of PAHs : isomerisation and dissociation.
- (7) Cami, J.; Bernard-Salas, J.; Peeters, E.; Elizabeth Malek, S. Detection of C60 and C70 in a Young Planetary Nebula. *Science* **2010**, *329*, 1180–1182.
- (8) Sellgren, K.; Werner, M. W.; Ingalls, J. G.; Smith, J. D. T.; Carleton, T. M.; Joblin, C. C60 in Reflection Nebulae. *Astrophys. J. Lett.* **2010**, *722*, L54.
- (9) Berné, O.; Mulas, G.; Joblin, C. Interstellar C60+. *Astron. Astrophys.* **2013**, *550*, L4.
- (10) Campbell, E. K.; Holz, M.; Gerlich, D.; Maier, J. P. Laboratory confirmation of C-60(+) as the carrier of two diffuse interstellar bands. *NATURE* **2015**, *523*, 322+.
- (11) Rauls, E.; Hornekær, L. Catalyzed Routes to Molecular Hydrogen Formation and Hydrogen Addition Reactions on Neutral Polycyclic Aromatic Hydrocarbons under Interstellar Conditions. *Astrophys. J.* **2008**, *679*, 531.
- (12) Bentarcourt, Y.; Ruetter, F.; Sánchez, M. Modeling formation of molecules in the interstellar medium by radical reactions with polycyclic aromatic hydrocarbons. *Int. J. Quant. Chem.* **2010**, *110*, 2560–2572.

- (13) Boschman, L.; Cazaux, S.; Spaans, M.; Hoekstra, R.; Schlathölter, T. H<sub>2</sub> formation on PAHs in photodissociation regions: a high-temperature pathway to molecular hydrogen. *Astron. Astrophys.* **2015**, *579*, A72.
- (14) Bouwman, J.; Cuppen, H. M.; Steglich, M.; Allamandola, L. J.; Linnartz, H. Photochemistry of polycyclic aromatic hydrocarbons in cosmic water ice II. Near UV/VIS spectroscopy and ionization rates. *Astron. Astrophys.* **2011**, *529*.
- (15) Hama, T.; Watanabe, N. Surface Processes on Interstellar Amorphous Solid Water: Adsorption, Diffusion, Tunneling Reactions, and Nuclear-Spin Conversion. *Chemical Reviews* **2013**, *113*, 8783–8839.
- (16) Thi, W.-F.; van Dishoeck, E. F.; Dartois, E.; Pontoppidan, K. M.; Schutte, W. A.; Ehrenfreund, P.; d’Hendecourt, L.; Fraser, H. J. VLT ISAAC 3.5  $\mu\text{m}$  spectroscopy of embedded young low mass stars III. Intermediate mass sources in Vela. *Astron. Astrophys.* **2006**, *449*, 251–265.
- (17) Bregman, J. D.; Hayward, T. L.; Sloan, G. C. Discovery of the 11.2 Micron Polycyclic Aromatic Hydrocarbon Band in Absorption toward Monoceros R2 IRS 3. *Astrophys. J. Lett.* **2000**, *544*, L75.
- (18) Chiar, J. E.; Tielens, A. G. G. M.; Whittet, D. C. B.; Schutte, W. A.; Boogert, A. C. A.; Lutz, D.; van Dishoeck, E. F.; Bernstein, M. P. The Composition and Distribution of Dust along the Line of Sight toward the Galactic Center. *Astrophys. J.* **2000**, *537*, 749.
- (19) Sellgren, K.; Brooke, T. Y.; Smith, R. G.; Geballe, T. R. A New 3.25 Micron Absorption Feature toward Monoceros R2/IRS 3. *Astrophys. J. Lett.* **1995**, *449*, L69.
- (20) Smith, R. G.; Sellgren, K.; Tokunaga, A. T. Absorption features in the 3 micron spectra of protostars. *Astrophys. J.* **1989**, *344*, 413–426.

- (21) Brooke, T. Y.; Sellgren, K.; Geballe, T. R. New 3 Micron Spectra of Young Stellar Objects with H<sub>2</sub>O Ice Bands. *Astrophys. J.* **1999**, *517*, 883.
- (22) Hardegree-Ullman, E. E.; Gudipati, M. S.; Boogert, A. C. A.; Lignell, H.; Allamandola, L. J.; Stapelfeldt, K. R.; Werner, M. Laboratory Determination of the Infrared Band Strengths of Pyrene Frozen in Water Ice: Implications for the Composition of Interstellar Ices. *Astrophys. J.* **2014**, *784*, 172.
- (23) Bernstein, M. P.; Sandford, S. A.; Allamandola, L. J. The Mid-Infrared Absorption Spectra of Neutral Polycyclic Aromatic Hydrocarbons in Conditions Relevant to Dense Interstellar Clouds. *Astrophys. J. Supp. Series* **2005**, *161*, 53.
- (24) Bouwman, J.; Mattioda, A. L.; Linnartz, H.; Allamandola, L. J. Photochemistry of PAHs in cosmic water ice I. Mid-IR spectroscopy and photoproducts. *Astron. Astrophys* **2011**, *525*, A93.
- (25) Osberg, K. I. Photochemistry and Astrochemistry: Photochemical Pathways to Interstellar Complex Organic Molecules. *Chem. Rev.* **2016**, *116*, 9631–9663, PMID: 27099922.
- (26) Bernstein, M. P.; Sandford, S. A.; Mattioda, A. L.; Allamandola, L. J. Near- and Mid-Infrared Laboratory Spectra of PAH Cations in Solid H<sub>2</sub>O. *Astrophys. J.* **2007**, *664*, 1264.
- (27) Bouwman, J.; Cuppen, H. M.; Bakker, A.; Allamandola, L. J.; Linnartz, H. Photochemistry of the PAH pyrene in water ice: the case for ion-mediated solid-state astrochemistry. *Astron. Astrophys.* **2010**, *511*.
- (28) Bouwman, J.; Paardekooper, D. M.; Cuppen, H. M.; Linnartz, H.; Allamandola, L. J. Real-Time Optical Spectroscopy of Vacuum Ultraviolet Irradiated Pyrene:H<sub>2</sub>O Interstellar Ice. *Astrophys. J.* **2009**, *700*, 56.



- (29) Bernstein, M. P.; Sandford, S. A.; Allamandola, L. J.; Gillette, J. S.; Clemett, S. J.; Zare, R. N. UV Irradiation of Polycyclic Aromatic Hydrocarbons in Ices: Production of Alcohols, Quinones, and Ethers. *Science* **1999**, *283*, 1135–1138.
- (30) Bernstein, M. P.; Dworkin, J. P.; Sandford, S. A.; Allamandola, L. J. Ultraviolet irradiation of naphthalene in H<sub>2</sub>O ice: Implications for meteorites and biogenesis. *Meteor. and Planet. Science* **2001**, *36*, 351–358.
- (31) Guennoun, Z.; Aupetit, C.; Mascetti, J. Photochemistry of coronene with water at 10 K: first tentative identification by infrared spectroscopy of oxygen containing coronene products. *Phys. Chem. Chem. Phys.* **2011**, *13*, 7340–7347.
- (32) Guennoun, Z.; Aupetit, C.; Mascetti, J. Photochemistry of Pyrene with Water at Low Temperature: Study of Atmospheric and Astrochemical Interest. *J. Phys. Chem. A* **2011**, *115*, 1844–1852.
- (33) Gudipati, M.; Allamandola, L. Polycyclic aromatic hydrocarbon ionization energy lowering in water ices. *Astrophys. J.* **2004**, *615*, L177–L180.
- (34) Woon, D.; Park, J. Photoionization of benzene and small polycyclic aromatic hydrocarbons in ultraviolet-processed astrophysical ices: A computational study. *Astrophys. J.* **2004**, *607*, 342–345.
- (35) Gudipati, M.; Allamandola, L. Unusual stability of polycyclic aromatic hydrocarbon radical cations in amorphous water ices up to 120 K: Astronomical implications. *Astrophys. J.* **2006**, *638*, 286–292.
- (36) Novakovskaya, Y. V.; Stepanov, N. F. Nonempirical Description of the Atmospherically Important Anionic Species. I. Water Cluster Anions. *Struct. Chem.* **2004**, *15*, 65–70.
- (37) Freidzon, A. Y.; Valiev, R. R.; Berezhnoy, A. A. Ab initio simulation of pyrene spectra in water matrices. *RSC Adv.* **2014**, *4*, 42054–42065.

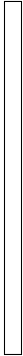
- (38) Sharma, D.; Sameera, W. M. C.; Andersson, S.; Nyman, G.; Paterson, M. J. Computational Study of the Interactions between Benzene and Crystalline Ice Ih: Ground and Excited States. *ChemPhysChem* **2016**, *17*, 4079–4089.
- (39) Michoulier, E.; Noble, J. A.; Simon, A.; Mascetti, J.; Toubin, C. Adsorption of PAHs on interstellar ice viewed by classical molecular dynamics. *Phys. Chem. Chem. Phys.* **2017**, *submitted*.
- (40) Gräfenstein, J.; Cremer, D. The self-interaction error and the description of non-dynamic electron correlation in density functional theory. *Theo. Chem. Acc. : Theo. Comp. Model.* **2009**, *123*, 171–182.
- (41) Porezag, D.; Frauenheim, T.; Köhler, T.; Seifert, G.; Kaschner, R. Construction of Tight-Binding-like Potentials on the Basis of Density Functional Theory - Application to Carbon. *Phys. Rev. B* **1995**, *51*, 12947–12957.
- (42) Seifert, G.; Porezag, D.; Frauenheim, T. Calculations of Molecules, Clusters, and Solids with a Simplified LCAO-DFT-LDA Scheme. *Int. J. Quantum Chem.* **1996**, *58*, 185–192.
- (43) Elstner, M.; Porezag, D.; Jungnickel, G.; Elsner, J.; Haugk, M.; Frauenheim, T.; Suhai, S.; Seifert, G. Self-consistent-charge density-functional tight-binding method for simulations of complex materials properties. *Phys. Rev. B* **1998**, *58*, 7260–7268.
- (44) Rapacioli, M.; Spiegelman, F.; Talbi, D.; Mineva, T.; Goursot, A.; Heine, T.; Seifert, G. Correction for dispersion and Coulombic interactions in molecular clusters with density functional derived methods: Application to polycyclic aromatic hydrocarbon clusters. *J. Chem. Phys.* **2009**, *130*, 244304–10.
- (45) Heine, T.; Rapacioli, M.; Patchkovskii, S.; Frenzel, J.; Koster, A.; Calaminici, P.; Duarte, H. A.; Escalante, S.; Flores-Moreno, R.; Goursot, A. et al. *deMonNano*, <http://demon-nano.ups-tlse.fr/> **2009**,

- (46) Rapacioli, M.; Simon, A.; Dontot, L.; Spiegelman, F. Extensions of DFTB to investigate molecular complexes and clusters. *Phys. Stat. Sol. B* **2012**, *249*, 245–258.
- (47) Li, J.; Zhu, T.; Cramer, C.; Truhlar, D. New Class IV Charge Model for Extracting Accurate Partial Charges from Wave Functions. *J. Phys. Chem. A* **1998**, *102*, 1820–1831.
- (48) Joalland, B.; Rapacioli, M.; Simon, A.; Joblin, C.; Marsden, C. J.; Spiegelman, F. Molecular Dynamics Simulations of Anharmonic Infrared Spectra of [SiPAH] pi-Complexes. *J. Phys. Chem. A* **2010**, *114*, 5846–5854.
- (49) Simon, A.; Rapacioli, M.; Mascetti, J.; Spiegelman, F. Vibrational spectroscopy and molecular dynamics of water monomers and dimers adsorbed on polycyclic aromatic hydrocarbons. *Phys. Chem. Chem. Phys.* **2012**, *14*, 6771–6786.
- (50) Simon, A.; Spiegelman, F. Water clusters adsorbed on polycyclic aromatic hydrocarbons: Energetics and conformational dynamics. *J. Chem. Phys.* **2013**, *138*.
- (51) Simon, A.; Spiegelman, F. Conformational dynamics and finite-temperature infrared spectra of the water octamer adsorbed on coronene. *Comput. Theor. Chem.* **2013**, *1021*, 54–61.
- (52) Oliveira, L. F. L.; Cuny, J.; Moriniere, M.; Dontot, L.; Simon, A.; Spiegelman, F.; Rapacioli, M. Phase changes of the water hexamer and octamer in the gas phase and adsorbed on polycyclic aromatic hydrocarbons. *Phys. Chem. Chem. Phys.* **2015**, *17*, 17079–17089.
- (53) Simon, A.; Noble, J. A.; Rouaut, G.; Moudens, A.; Aupetit, C.; Iftner, C.; Mascetti, J. Formation of coronene: water complexes: FTIR study in argon matrices and theoretical characterisation. *Phys. Chem. Chem. Phys.* **2017**, *19*, 8516–8529.

- (54) Temelso, B.; Archer, K. A.; Shields, G. C. Benchmark Structures and Binding Energies of Small Water Clusters with Anharmonicity Corrections. *J. Phys. Chem.A* **2011**, *115*, 12034–12046.
- (55) Rapacioli, M.; Spiegelman, F.; Scemama, A.; Mirtschink, A. Modeling Charge Resonance in Cationic Molecular Clusters: Combining DFT-Tight Binding with Configuration Interaction. *J. Chem. Theo. Comp.* **2011**, *7*, 44–55.
- (56) Rapacioli, M.; Spiegelman, F. Modelling singly ionized coronene clusters. *Eur. Phys. J. D* **2009**, *52*, 55–58.
- (57) Simon, A.; Rapacioli, M.; Rouaut, G.; Trinquier, G.; Gadéa, F. X. Dissociation of polycyclic aromatic hydrocarbons: molecular dynamics studies. *Phil. Trans. Roy. Soc. A* **2017**, *375*.
- (58) Widmark, P.-O.; Malmqvist, P.-Å.; Roos, B. O. Density matrix averaged atomic natural orbital (ANO) basis sets for correlated molecular wave functions. *Theor. Chim. acta* **1990**, *77*, 291–306.
- (59) Aquilante, F.; De Vico, L.; Ferré, N.; Ghigo, G.; Malmqvist, P.-å.; Neogrady, P.; Pedersen, T. B.; Pitoňák, M.; Reiher, M.; Roos, B. O. et al. MOLCAS 7: The Next Generation. *J. Comput. Chem.* **2010**, *31*, 224–247.
- (60) Karlström, G.; Lindh, R.; Malmqvist, P.-Å.; Roos, B. O.; Ryde, U.; Veryazov, V.; Widmark, P.-O.; Cossi, M.; Schimmelpfennig, B.; Neogrady, P. et al. MOLCAS: a program package for computational chemistry. *Comput. Mat. Science* **2003**, *28*, 222–239.
- (61) Veryazov, V.; Widmark, P.-O.; Serrano-Andrés, L.; Lindh, R.; Roos, B. O. 2MOLCAS as a development platform for quantum chemistry software. *Int. J. Quantum Chem.* **2004**, *100*, 626–635.

- (62) Sugita, Y.; Okamoto, Y. Replica-Exchange Molecular Dynamics Method for Protein Folding. *Chem. Phys. Lett.* **1999**, *314*, 141–151.
- (63) Korchagina, K. A.; Simon, A.; Rapacioli, M.; Spiegelman, F.; Cuny, J. Structural Characterization of Sulfur-Containing Water Clusters Using a Density-Functional Based Tight-Binding Approach. *J. Phys. Chem. A* **2016**, *120*, 9089–9100.
- (64) Burke, D. J.; Brown, W. A. Ice in space: surface science investigations of the thermal desorption of model interstellar ices on dust grain analogue surfaces. *Phys. Chem. Chem. Phys.* **2010**, *12*, 5947–5969.
- (65) Bahr, S.; Kempter, V. Interaction of benzene with amorphous solid water adsorbed on polycrystalline Ag. *J. Chem. Phys.* **2007**, *127*, 074707.
- (66) Thrower, J. D.; Collings, M. P.; Rutten, F. J. M.; McCoustra, M. R. S. Thermal desorption of  $C_6H_6$  from surfaces of astrophysical relevance. *The Journal of Chemical Physics* **2009**, *131*, 244711.
- (67) Stubbing, J.; Salter, T.; Brown, W. *private communication*
- (68) Noble, J. A.; Jouvét, C.; Aupetit, C.; Moudens, A.; Mascetti, J. Efficient photochemistry of coronene:water complexes. *Astron. Astrophys.* **2017**, *599*, A124.
- (69) Cuppen, H. M.; Walsh, C.; Lamberts, T.; Semenov, D.; Garrod, R. T.; Penteado, E. M.; Ioppolo, S. Grain Surface Models and Data for Astrochemistry. *Space Science Rev.* **2017**, *212*, 1–58.

# TOC Graphic



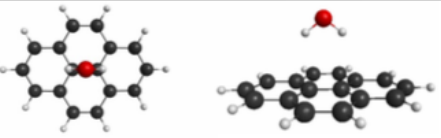
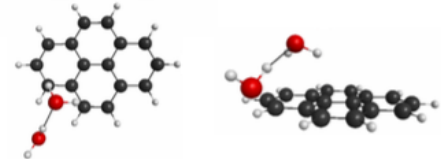
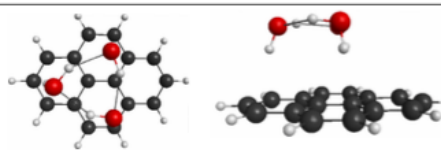
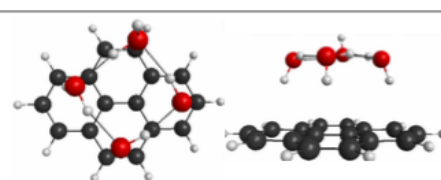
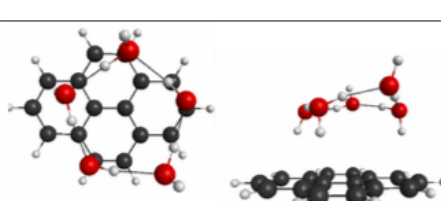
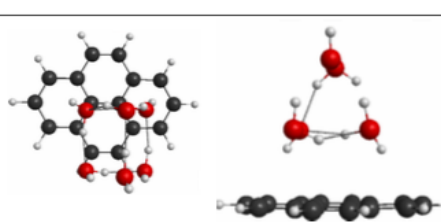
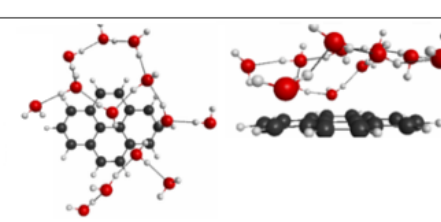
# H <sub>2</sub> O	IP (eV) MP2 / C-DFTB/DFTB	DFTB optimized structures
1	7.62 / 7.63 / 7.61 (0.91)	
2	7.52 / 7.49 / 7.44 (0.90)	
3	7.91 / 7.86 / 7.77 (0.80)	
4	7.84 / 7.76 / 7.66 (0.77)	
5	7.80 / 7.69 / 7.57 (0.75)	
6	7.70 / 7.64 / 7.49 (0.76)	
13	7.54 / 7.50 / 7.14 (0.57)	

Figure 1: DFTB most stable geometries of water-pyrene clusters ( $n_{H_2O}=1-6, 13$ ) found following the method described in section 2.2, and computed VIP's values at the C-DFTB, DFTB and MP2 levels of theory. The number in parenthesis indicate the partial charge on the pyrene entity, within the molecular cation, at the geometry of the optimised neutral cluster, with the DFTB approach.

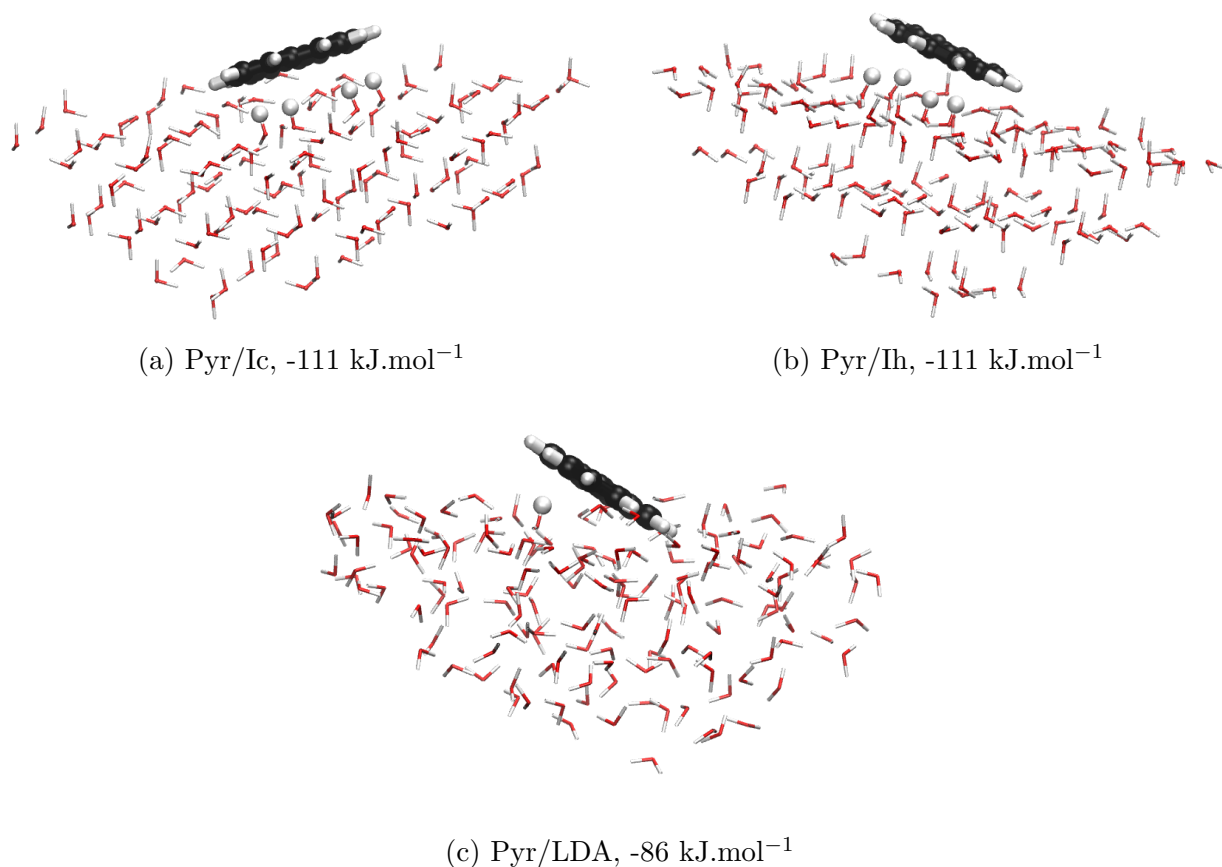


Figure 2: DFTB optimized pyr/ice geometries when  $E_{\text{int}}(\text{pyr/ice})$  is minimum for the three ices Ic (a), Ih (b) and LDA (c). The interaction energy for each configuration is reminded below each represented structure. The OH dangling bonds are represented with white balls.

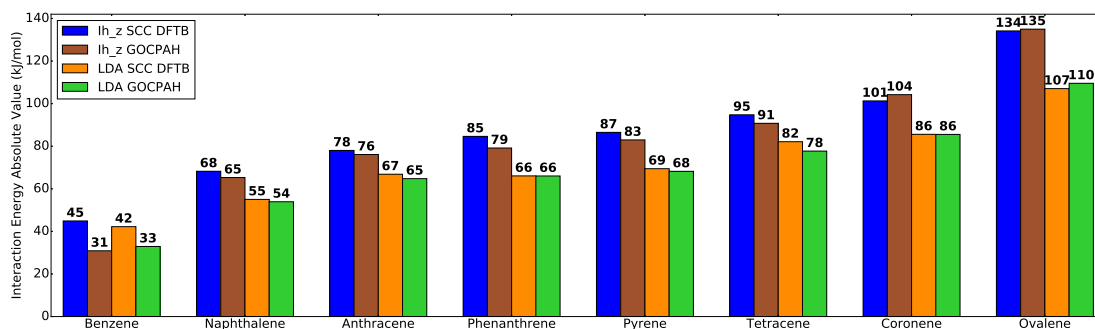


Figure 3: PAH-ice interaction energies (absolute values) : comparison between DFTB and FF (GOCPAH) values



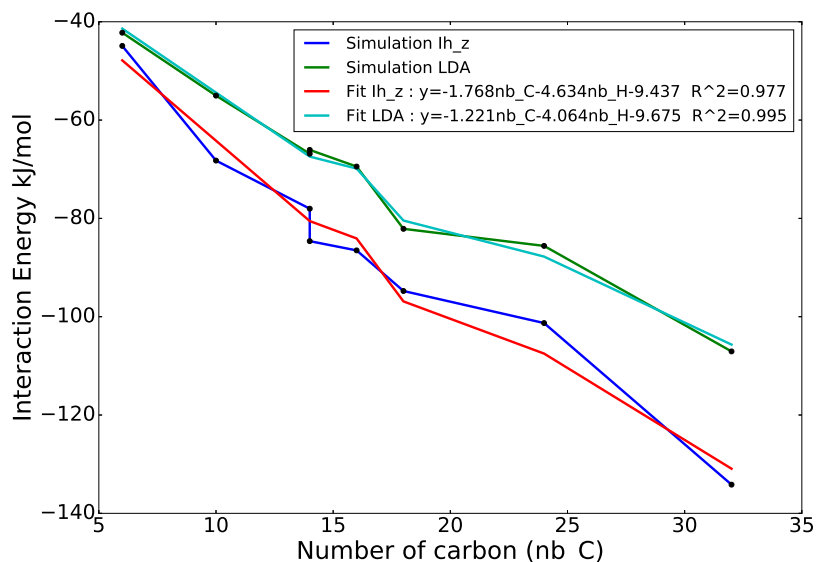


Figure 4: First order dependence of DFTB PAH-ice adsorption energy on the numbers of C and H atoms as a function of the number of C atoms for Ih (red) and LDA (green) ices. **IL FAUT EXPLIQUER CE QU'EST R2 DANS LA LEGENDE.**

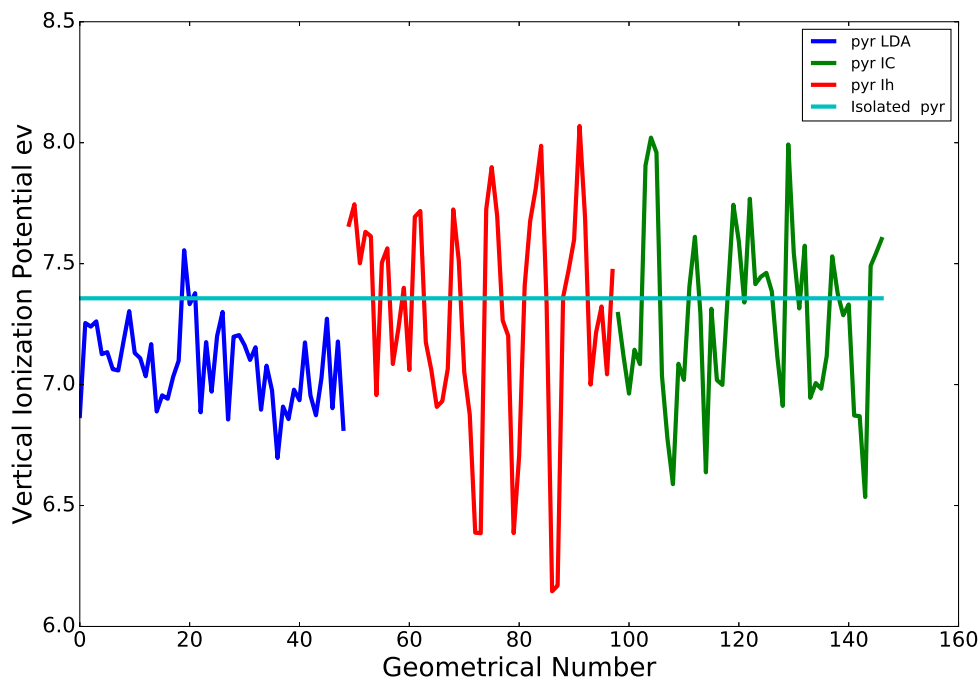


Figure 5: C-DFTB vertical ionisation potential of pyrene adsorbed on water ice for the 50 optimized DFTB geometries (blue : LDA, red : Ih, green: IC, cyan: bare pyrene)

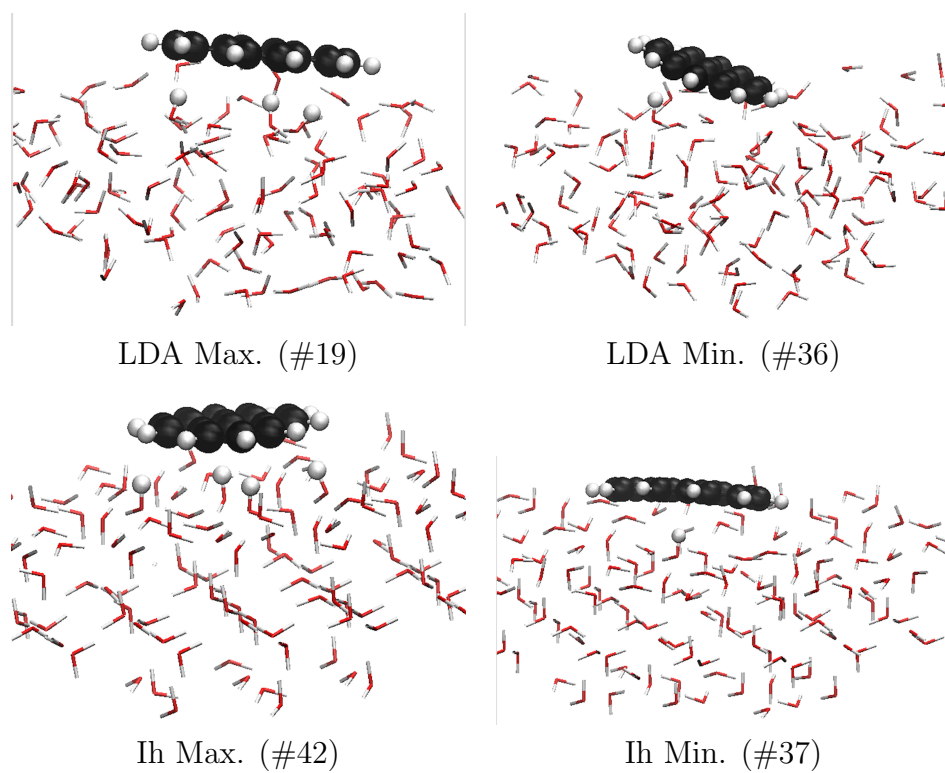


Figure 6: Geometries corresponding to the configuration numbers reported in Figure 3 **Fig5** (number in parenthesis) that lead to the maximum (Max) or minimum (Min) IP. The H of the dangling OH pointing towards the PAH are represented with balls.

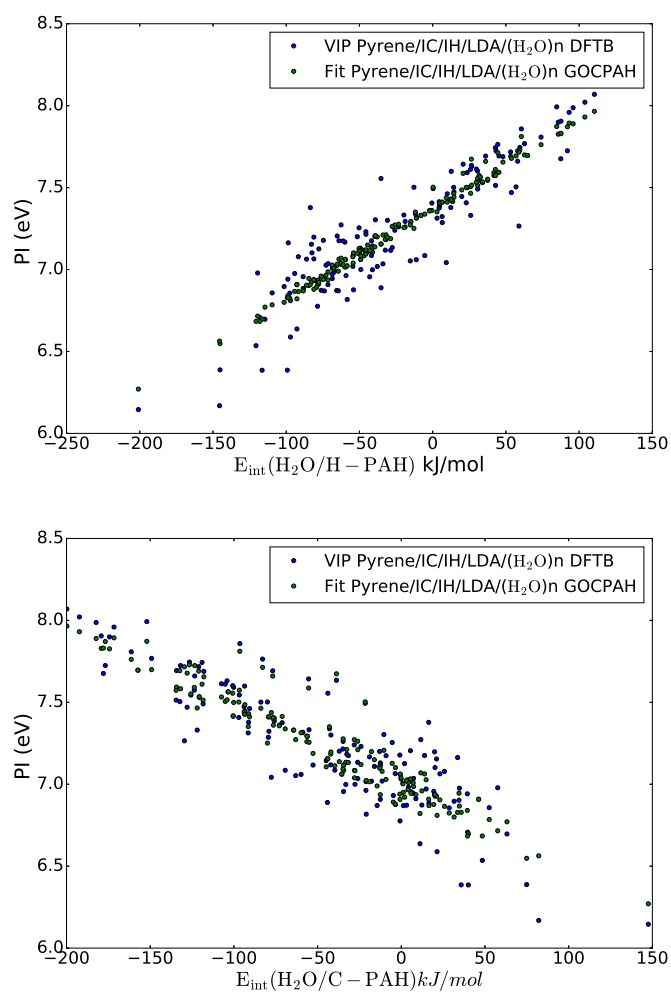
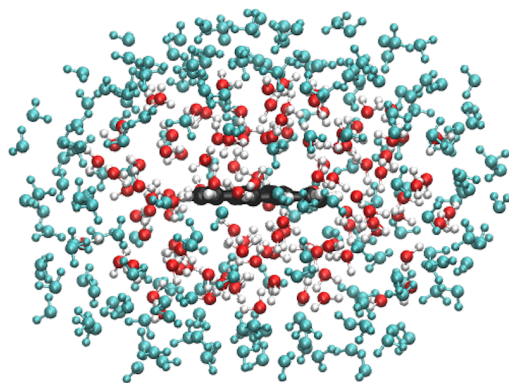
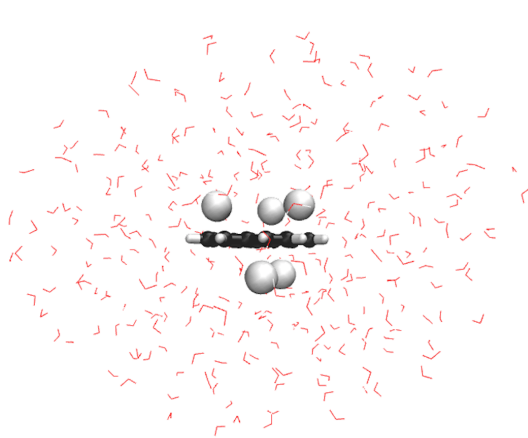


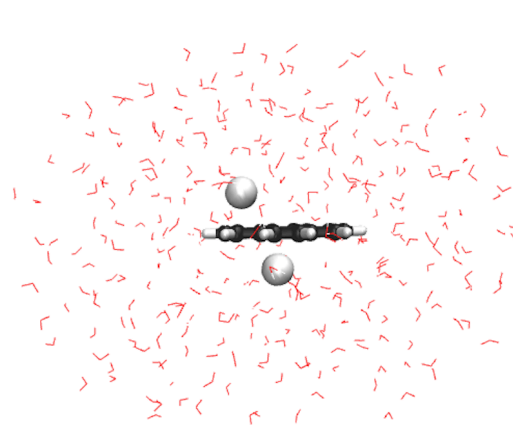
Figure 7: Correlation laws established between VIP values (C-DFTB) and pair interaction energies (GOCPAH force field).



(a) Example of solvated pyrene. The molecules in blue are frozen, the others are relaxed during the optimization.



(b) Configuration 1 of solvated pyrene for which the interaction energy is  $-163 \text{ kJ.mol}^{-1}$ . The VIP is  $7.29 \text{ eV}$ .



(c) Configuration 2 of solvated pyrene for which the interaction energy is  $-152 \text{ kJ.mol}^{-1}$ . The VIP is  $7.04 \text{ eV}$ .

Figure 8: Solvated pyrene geometries. Dangling OH bonds of water molecules interacting with carbons are represented with white balls. Configuration 1 (resp. 2) contains 122 (resp. 116) water molecules allowed to relax during the relaxation process), and 201 (resp. 206) frozen water molecules.